Journal of Power Sources 240 (2013) 510–514

Contents lists available at SciVerse ScienceDirect

Journal of Power Sources

journal homepage: www.elsevier.com/locate/jpowsour

Short communication

All-solid secondary batteries with sulfide-based thin film electrolytes

Takashi Uemura*, Kazuhiro Goto, Mitsuyasu Ogawa, Keizo Harada

Sumitomo Electric Industries, Ltd., Electronics & Materials R&D Laboratories, Koyakita, Itami, Hyogo 664-0016, Japan

HIGHLIGHTS

- All-solid batteries with sulfide-based thin film electrolyte has been investigated.
- The battery has shown discharge of 10 C for 1 min at a room temperature.
- The battery has shown excellent cycle properties at a high temperature.

ARTICLE INFO

Article history:
Received 25 January 2013
Received in revised form
9 April 2013
Accepted 12 April 2013
Available online 23 April 2013

Keywords:
All-solid secondary battery
Sulfide-based solid electrolyte
High-rate discharge
Cycle performances at high temperature
Degradation mechanisms at high temperature

ABSTRACT

We have been developing all-solid secondary batteries with sulfide-based thin film electrolyte and pellet-type electrodes. This battery has high performance – it has high-rate discharge properties and cycle properties at high temperature. The battery has shown discharge capability of 10 C for 1 min and cycle properties of 90% capacity-1500 cycle at 60 °C, 90% capacity-500 cycle at 80 °C, and 70% capacity-500 cycle at 150 °C. It has been found that thin film electrolyte gives good effect on both high-rate discharge and cycle performance at a high temperature.

1. Introduction

Secondary batteries are widely used to power mobile electronic devices and other equipment, and extensive research has led to the development of lithium-ion batteries with a high energy density. As a larger number of vehicles use lithium-ion batteries, it has become increasingly important to improve their safety. However, lithium-ion batteries, which use combustible organic electrolyte solutions, have ignition and explosion risk. To address this problem, efforts are currently underway to significantly increase the safety of lithium-ion batteries by replacing the electrolyte solutions with flame-retardant electrolytes [1–3]. Among others, an all-solid lithium secondary battery, which has a high thermal stability from room temperature to 360 °C [3] and can operate using Li_2S–P_2S_5 sulfide solid electrolytes with a high lithium-ion conductivity of at least 1×10^{-3} S cm^{-1} at room temperature [4], is receiving particular attention as a next-generation rechargeable battery. However, all-solid batteries using no organic electrolyte solutions have the following problems: it is difficult to ensure a wide contact area at the interface between the active material and electrolyte; a significantly low mobility of lithium ions at the contact interface between the cathode material and solid electrolyte increases the interface resistance, which affects the power density of the battery [5–7]. The first problem concerning the contact .area is particularly serious with bulk-type, all-solid batteries; it is necessary to apply a strong press force to the electrode during its evaluation, which has been an obstacle to its practical use. Regarding the second problem, you can effectively reduce the interface resistance by coating the surface of the cathode material with a film of lithium-ion conductive oxide to create a buffer layer (interlayer) [8]. Thinning the solid electrolyte layer between the positive and negative-electrode to reduce the interface resistance also effectively improves the high-rate charge and discharge performance. We produced a prototype all-solid-state battery consisting of laminated layers of positive- and negative-electrode materials and a solid electrolyte, and the solid electrolyte thin film layer of the battery maintained its performance during charging and discharging with a cycle of 500 [9–

* Corresponding author. Tel.: +81 72 771 3137; fax: +81 72 771 3239.
E-mail addresses: uemura-takashi@sei.co.jp (T. Uemura), gotou-kazuhiro@sei.co.jp (K. Goto), ogawa-mitsuyasu@sei.co.jp (M. Ogawa), harada-keizo@sei.co.jp (K. Harada).

0378-7753/$ – see front matter © 2013 Elsevier B.V. All rights reserved.
http://dx.doi.org/10.1016/j.jpowsour.2013.04.060

11]. All-solid-state lithium cells using a sulfide thin film electrolyte as a separator to the powder composite electrodes also has been reported [12].

We produced a new structured prototype of the all-solid battery with a sulfide solid electrolyte film by the vapor-phase method, between the bulk electrodes consisting of a mixture of powders. Because of the preparation of thin film electrolytes on both of cathode and anode before attaching electrodes, the defects that penetrate through the electrolyte layer were reduced. Additionally, it is possible to use the "rocking chair" type active material on both electrodes. As a result, short circuiting was reduced, and we succeeded in achieving the high-rate discharge and cycle (at a high temperature). The present study reports the assessment results.

2. Experimental

2.1. Preparation of electrode materials

The commercial $LiNi_{0.8}Co_{0.15}Al_{0.05}O_2$ (Toda Kogyo Corp.) and 2 wt% carbon-added $Li_4Ti_5O_{12}$ (Ishikawa Sangyo Kaisha, Ltd.) were used for the cathode and anode materials, respectively, and Li_2S–P_2S_5 glass ceramic powder as a solid electrolyte. A mixture of active material and solid electrolyte powders was used as electrode materials: a $80Li_2S$–$20P_2S_5$ solid electrolyte with an Li:P molar ratio of 8:2 or a $70Li_2S$–$30P_2S_5$ solid electrolyte with an Li:P molar ratio of 7:3 for the positive-electrode, and a $70Li_2S$–$30P_2S_5$ solid electrolyte for the negative-electrode. The synthetic condition of these electrolyte powders is shown in previous reports [13].

The cathode materials contained in all samples were coated with $LiNbO_3$, which serves as an intermediate layer. The intermediate layer was created using "Coating Equipment for Rolling Fluidized Beds MP-01" (Powrex Corp.) – the same method reported on in a study conducted by Takada et al. [8]. An alkoxide solution of metallic elements was used as the material for the intermediate layer; an ethanol solution containing 5 wt% of lithium ethoxide (structural formula: $Li(OC_2H_5)$) was used as the lithium source; pentaethoxyniobium (structural formula: $Nb(OC_2H_5)_5$, purity of 4N) was used as the niobium source. A mixture of an ethanol solution containing 5 wt% of lithium ethoxide and pentaethoxyniobium with a prescribed ratio was sprayed at 500 g of $LiNi_{0.08}Co_{0.15}Al_{0.05}O_2$ poured into the equipment at a temperature of 80 °C at 1 g min^{-1} to create the coating, which then underwent heat treatment for 30 min at 300 °C to create the intermediate layer of $LiNbO_3$. Inductively Coupled Plasma Atomic Emission Spectroscopy (ICP-AES, iCAP6500DUO, Thermo Fisher Scientific) was performed to determine the ratio of elements contained in the intermediate layer and cathode material. Field Emission Auger Electron Spectroscopy (FE-AES, PHI700, ULVAC-PHI, INC.) was also performed to examine changes in the particle surface during coating, using an electron gun with an accelerating voltage of 10 keV. All of the batteries used for electrochemical measurements were made from the same processed $LiNi_{0.08}Co_{0.15}Al_{0.05}O_2$. No intermediate layer was formed in the anode material.

2.2. Process of forming bulk electrodes

Table 1 shows the mixture ratios of active materials/SE and pressurized conditions. No addictive carbons were mixed. Mixed powders were put into a mold and pressed in a dry room with a dew point of −55 °C. The electrodes were cut cross-sectionally using a focused ion beam system to observe the inside with scanning ion microscopy (FIB-SIM, FB2100, Hitachi, Ltd.). The electrodes for the batteries were prepared except for the electrodes for the analysis of FIB and SIM. When creating electrodes, aluminum plates were also pressed as power collectors.

Table 1
Materials and press condition of bulk-type electrodes.

	Electrode weight ratio (active material:electrode)	Active material weight	Press condition
Cathode	70 wt%:30 wt%	19.4 mg cm^{-2}	540 MPa × 10 min
Anode	60 wt%:40 wt%	18.8 mg cm^{-2}	540 MPa × 10 min

2.3. Preparation of electrolyte films

Solid electrolyte film was formed on both the positive and negative bulk electrodes. Using a vacuum deposition below 0.005 Pa, 5-μm solid electrolyte film was formed, with Li_2S and P_2S_5 as the starting materials. The sides of the sulfide solid electrolyte films of positive and negative bulk electrodes were put together and pressure of 16 MPa was applied to integrate the electrolytes. The bulk electrolytes were attached together over an area of φ10 mm, based on which the density of the battery capacity was calculated.

2.4. Evaluation of charge and discharge properties

Only constant-current, charge–discharge tests using a BLS battery test system (Keisokuki Center Co., Ltd.) were conducted to examine the high-rate discharge and cycle characteristics of the batteries. Prior to and following charging, an alternating-current impedance measurement using an analyzer (ALS model 6005C, BAS Inc.) was conducted under the following conditions: an alternating-current amplitude of 10 mV and a frequency range of 10 mHz–100 kHz.

3. Results and discussion

3.1. Evaluation of electrode

After coating the cathode powder $LiNi_{0.8}Co_{0.15}Al_{0.05}O_2$ with $LiNbO_3$, an intermediate layer, ICP analysis was conducted to determine the ratio of elements; the weight of Ni and Nb contained in 100 mg of coated powder was 48 and 0.85 mg, respectively. The mean thickness, calculated based on a specific surface area of the powder (0.41 m^2 g^{-1}) determined by the conventional gas absorption method and the theoretical density of the intermediate layer, was 7.2 nm. The results of the element mapping in Fig. 1, obtained using Auger spectroscopy, estimated the surface coverage of the intermediate layer $LiNbO_3$ to be approximately 80%. Previous studies reported that, regarding all-solid batteries, the thickness of the intermediate layer $LiNbO_3$ or $Li_4Ti_5O_{12}$ for the cathode material $LiCoO_2$ should be 5–7 nm [5,6], and the intermediate layer $Li_4Ti_5O_{12}$ for $LiNi_{0.8}Co_{0.15}Al_{0.05}O_2$ should be approximately 5 nm [8]. The thickness of the intermediate layer $LiNbO_3$ for $LiNi_{0.8}Co_{0.15}Al_{0.05}O_2$ reported in the present study is in line with the results of previous studies.

The FIB-SIM sectional image in Fig. 2 shows that the inside of the pressed electrodes in molds was dense, and that there was a close contact between the cathode and anode materials and solid electrolytes. Primary particles of 1 μm or smaller and secondary particles of approximately 6 μm were observed in both active materials. Even-grain boundaries were barely visible between the solid electrolyte particles, and the contact resistance was considered to be markedly low.

3.2. Charge and discharge performance

An examination was conducted on the charge and discharge characteristics of the battery that used an $80Li_2S$–$20P_2S_5$ solid

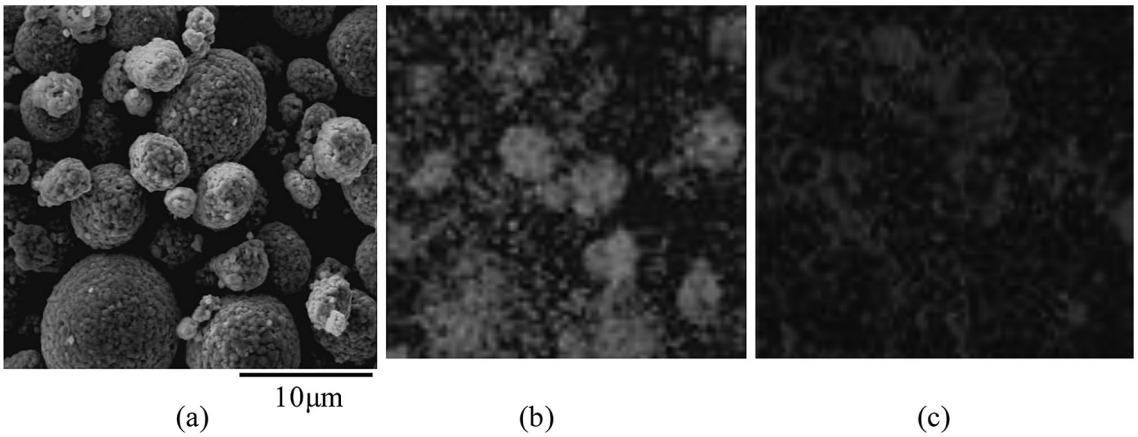

Fig. 1. SEM image of $LiNi_{0.8}Co_{0.15}Al_{0.05}O_2$ powder after coating the $LiNbO_3$ intermediate layer: a) and the images of element mapping with Auger spectroscopy: b) is Nb mapping image, and c) is Ni mapping image.

electrolyte as a positive-electrode material, and a $70Li_2S{-}30P_2S_5$ solid electrolyte as a negative-electrode material. The battery was charged at 0.1 C (0.3 mA cm^{-2}) at a room temperature of 25 °C, and discharged at a different current value. Fig. 3 shows the results – the horizontal was normalized by the weight of positive active material. With a current density of as high as 10 C (30 mA cm^{-2}), the battery was able to discharge for 15 s, and the discharge capacity was 6.4 mAh g^{-1}.

The battery that used $70Li_2S{-}30P_2S_5$ solid electrolytes for both positive- and negative-electrode materials was charged at a room temperature of 25 °C at 0.1 C (0.3 mA cm^{-2}), and discharged at a different current value. Fig. 4 shows the results. At the time of discharge at a high-rate (5 and 10 C), the battery capacity was higher, compared to a cell using an $80Li_2S{-}20P_2S_5$ solid electrolyte on the positive-electrode side: the battery was able to discharge for 1 min at 10 C (0.3 mA cm^{-2}), and the discharge capacity was 25.7 mAh g^{-1}. The solid electrolyte in the form of pressurized powder was examined to evaluate its ionic conductivity. The measured ionic conductivity of $70Li_2S{-}30P_2S_5$ pellet was 1×10^{-3} (S cm^{-1}) – higher than the ionic conductivity of $80Li_2S{-}20P_2S$ pellet: 4×10^{-4} (S cm^{-1}), which suggested an increase in the capacity.

3.3. Cycle performance at high temperature

A battery that used an $80Li_2S{-}20P_2S_5$ solid electrolyte as a positive-electrode material and a $70Li_2S{-}30P_2S_5$ solid electrolyte as a negative-electrode material was packaged into a 2032 coin cell. Fig. 5 shows the results of a charge–discharge test on a coin cell battery. The coulomb efficiency in the first and second cycles was 73% and 94%, respectively, and the discharge capacity was 148 mAh g^{-1}. Except for an outside package the battery was fabricated with the same process as Fig. 3 battery. It was supposed that the slight difference of capacity between Figs. 3 and 5 was due to a small difference of the dispersion of active material powder in the electrodes.

The battery was charged and discharged in cycles by applying a 3V–1V cut-off voltage at 60 °C and 3 mA cm^{-2}, and Fig. 6 shows the capacity change during the charge and discharge cycles. The discharge capacity was the highest, 149 mAh g^{-1} (100%), in the fifth cycle, 143 mAh g^{-1} (96%) at the end of the 500th cycle, 137 mAh g^{-1} (92%) at the end of the 1000th cycle, and 134 mAh g^{-1} (90%) at the end of the 1500th cycle. Fig. 7 is detailed information on discharge rate property at a room temperature. The battery is the same in Figs. 6 and 7. The discharge capacity was measured after cooling to room temperature at the end of the 500th cycle and 1000th cycle at 60 °C. As a result, the capacity at discharge current of 3 mA cm^{-2}

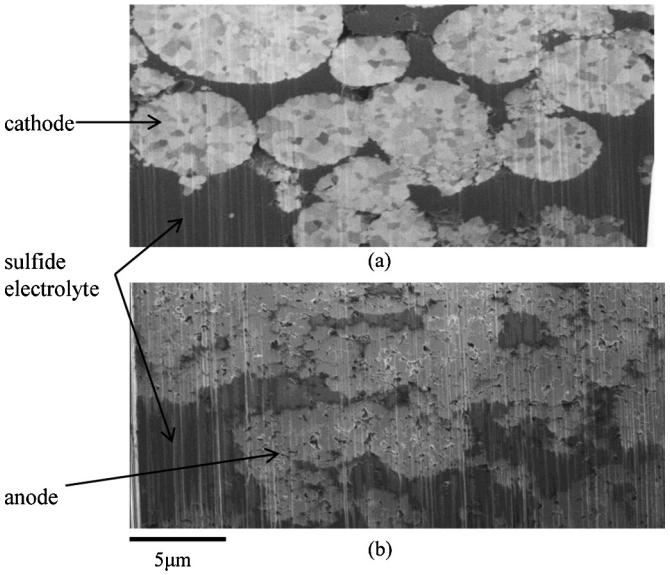

Fig. 2. FIB-SIM sectional images shown that the inside of the pressed electrodes: a) positive-electrode, and b) negative-electrode.

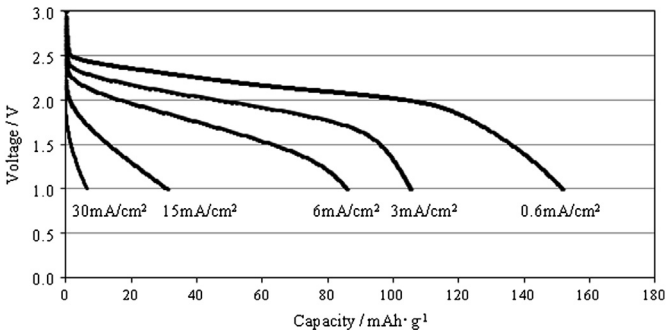

Fig. 3. Discharge curves at various current density of a battery that used an $80Li_2S{-}20P_2S_5$ solid electrolyte as a positive-electrode, and a $70Li_2S{-}30P_2S_5$ solid electrolyte as a negative-electrode.

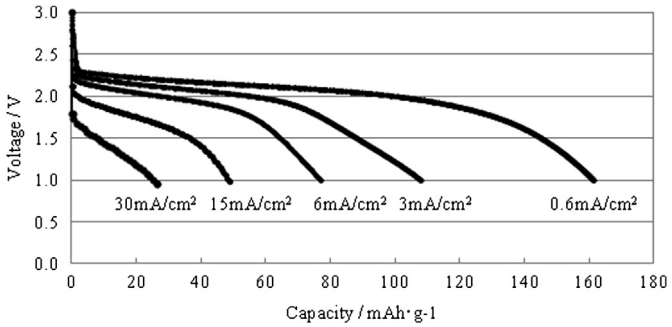

Fig. 4. Discharge curves at various current of a battery that used a $70Li_2S{-}30P_2S_5$ solid electrolyte as a positive and negative electrodes.

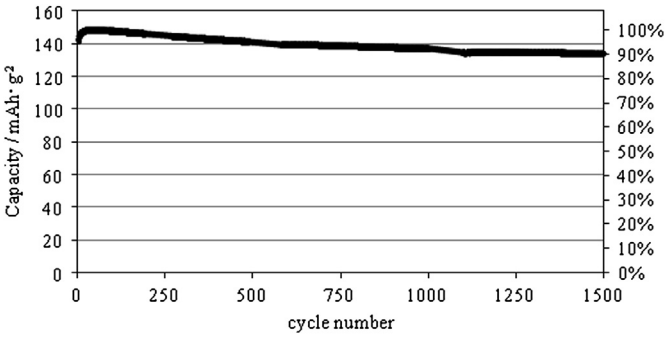

Fig. 6. Charge and discharge cycle performance of the coin cell at 60 °C.

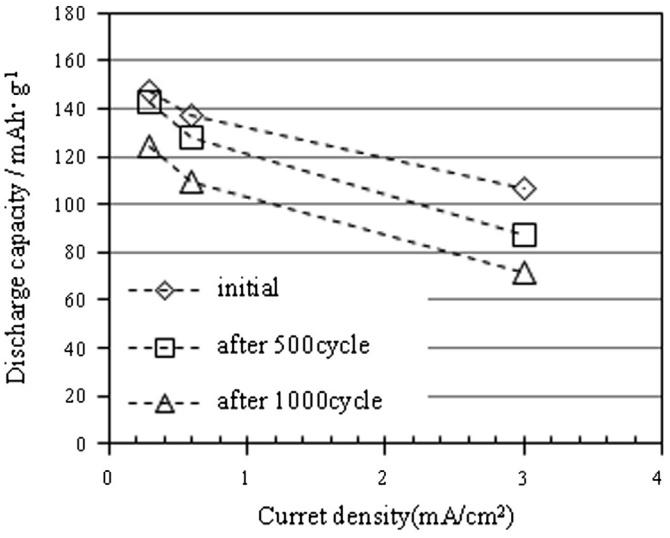

Fig. 7. Discharge capacity at 25 °C after 60 °C charge and discharge cycles.

declined to approximately 60% of the initial capacity after the 1000th cycle. The Nyquist plot in Fig. 8 shows impedance measured immediately after the evaluation of these characteristics of discharge capacity; there were no significant changes in the resistance component: R_1, and a moderate increase in the resistance component: R_2. It was appropriate to consider that the resistance component at higher frequencies (R_1) was the resistance of the solid electrolyte, and that the resistance component at lower frequencies (R_2) was a charge-transfer reaction at the interface. However, the value of the resistance of electrolyte was estimated below 3 ohm cm^{-2} from the ionic conductivity and thickness of an electrolyte layer. The estimated value was smaller than the measured R_1. It is supposed that this difference would be due to the addition of the electronic resistance of the battery in R_1 value. In detail R_2 seems to consist of two capacitance components, and the resistance of the higher frequency component increased after the cycle test. The R_2 of the battery using $LiNbO_3$ non-coated positive active material was ten times larger than the R_2 of Fig. 9. It is supposed that the two components of R_2 belong to the two interfaces of cathode/electrolyte and anode/electrolyte. This suggests that the cause of the decrease in the discharge capacity was increased resistance in the active material and at the interface of the solid electrolyte, and that the ionic conductivity of the solid electrolyte film remained as it was at the initial state.

Previous studies on degradation mechanisms at high temperature report that different phases are formed at the interface between the cathode material and sulfide solid electrolyte, which significantly increases the interface resistance [14]. To examine the formation of different phases at the interface, a battery with the same structure as the above-mentioned battery was charged and discharged through 500 cycles at 60 °C, and TEM-EDX analysis of the interface between the cathode material and solid electrolyte was conducted. As shown in Fig. 9, there was no different phase at the interface, although a small amount of oxygen was observed at the interface of the solid electrolyte. The initial sample fabricated by the same process as the battery in Fig. 9 showed no oxygen at the interface of the solid electrolyte, based on the TEM-EDX method. So, it was supposed that oxygen at the interface dispersed from the active material. Oxygen was released from the active material which became unstable because of an overcharge of part of the cathode materials, impurities, and other factors. The oxygen dispersion at the interface was considered to have increased the

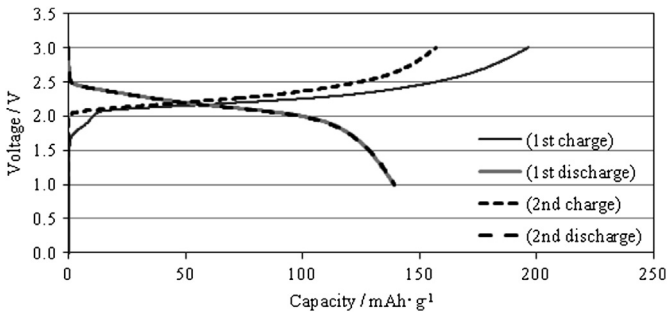

Fig. 5. Charge–discharge performance of the coin cell battery.

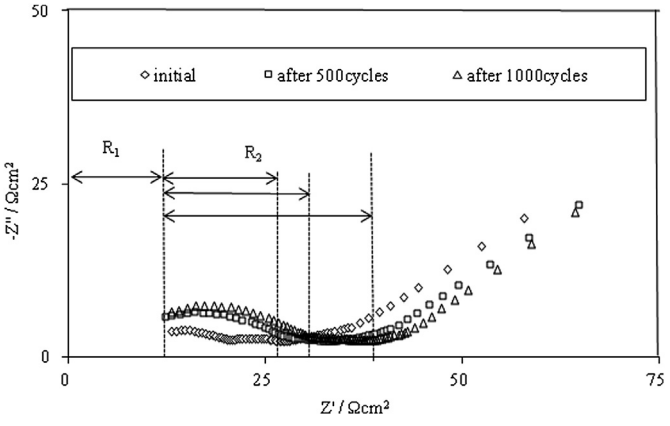

Fig. 8. Nyquist plot measured at 25 °C after 60 °C charge and discharge cycles.

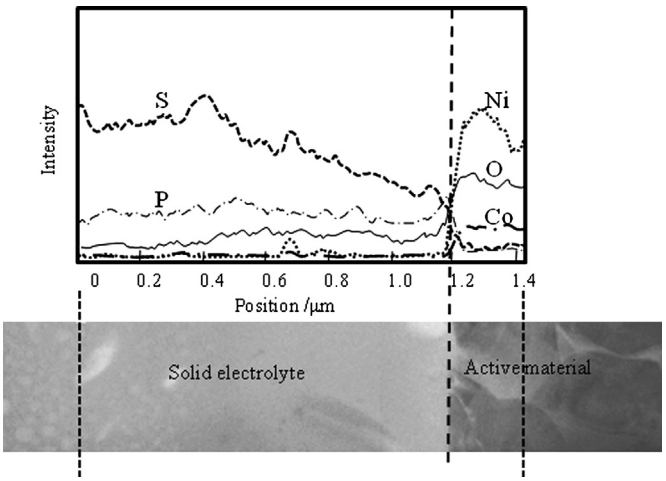

Fig. 9. TEM-EDX analysis of the interface between $80Li_2S{-}20P_2S_5$ solid electrolyte and $LiNi_{0.8}Co_{0.15}Al_{0.05}O_2$ after the 500th cycle at 60 °C.

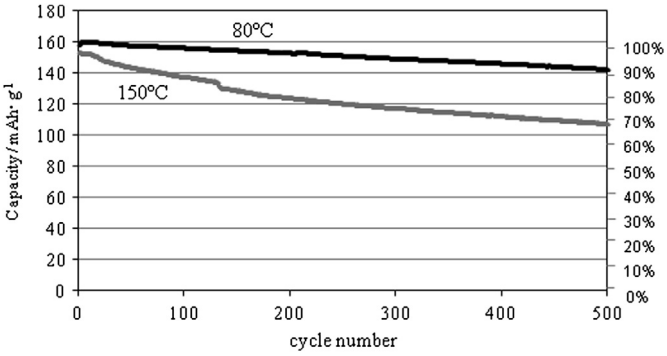

Fig. 10. Charge and discharge cycle performance of the coin cell at 80 °C and 150 °C.

resistance component R_2 and decreased the discharge capacity following the cycle test at 60 °C. The formation of an inter-particle void due to a change in the volume of the active material during charge and discharge was also considered to be a physical factor related to an increase in the resistance at the interface. However, since the change in the volume of the anode material $Li_4Ti_5O_{12}$, in particular, was only 0.2% when the SOC was between 0 and 100% [15], and as shown in Fig. 9, chemical degradation was the primary cause.

No previous studies reported that the high discharge rates and long-term cycle characteristics shown in Figs. 6 and 7 could be compatible, although a moderate level of high temperature degradation was noted. This compatibility was achieved because: the volume of the active material did not significantly change during charge and discharge, and the electrodes and solid electrolyte films created using the vacuum evaporation method were dense.

A test involving an all-solid battery that used an $80Li_2S{-}20P_2S_5$ solid electrolyte on the positive side was also conducted to examine changes in its discharge capacity while the battery was charged and discharged in cycles at 80 and 150 °C. In the cycle test, the current value was 3 mA cm^2 and the cut-off voltage was 3 V–1 V when the temperature was 80 °C; and the current value was 9 mA cm^{-2} and the cut-off voltage was 2.7 V–1 V when the temperature was 150 °C. Fig. 10 shows the results of the test conducted at high temperature; the initial discharge capacity was 158 mAh g^{-1} (100%) and 142 mAh g^{-1} (90%) at the end of the 500th cycle when the temperature was 80 °C; the initial discharge capacity was 155 mAh g^{-1} (100%) and 108 mAh g^{-1} (70%) at the end of the 500th cycle at 150 °C, which suggests that the battery has a driving power of 500 cycles of charge and discharge at 150 °C.

4. Conclusion

In recent years, several advanced studies have reported that all-solid batteries have the ability to discharge at a high current density [8,16]. The battery examined in the present study demonstrated a higher capacity and high-rate discharge performance at room temperature and more favorable cycle characteristics, compared to batteries reported in previous studies. Although several studies have been conducted to examine the heat resistance of all-solid batteries according to their constituents, there are few reports on the integrated driving characteristics of batteries. The present study demonstrated that all-solid batteries can be charged and discharged in 500 cycles at 150 °C or in a harsh temperature environment. These battery characteristics achieved a decrease in the interface resistance by coating the intermediate layer in a cathode material and a reduction in the bulk resistance using thin film as solid electrolyte layer.

Acknowledgment

Lastly we would like to convey our thanks to Idemitsu Kosan Co., Ltd. for providing us with the solid electrolyte powder required in the present study as a material for electrodes.

References

[1] K. Takada, N. Aotani, K. Iwamoto, S. Kondo, Solid State Ionics 86 (1996) 877–882.
[2] R. Hagiwara, K. Tamaki, K. Kubota, T. Goto, T. Nohira, J. Chem. Eng. Data 53 (2008) 355.
[3] A. Hayashi, J. Ceram. Soc. Jap. 115 (2007) 110–117.
[4] N. Kayama, K. Homma, Y. Yamakawa, M. Hirayama, R. Kanno, M. Yonemura, T. Kamiyama, Y. Kato, S. Hama, K. Kawamoto, A. Mitsui, Nat. Mater. 10 (2011) 682–686.
[5] N. Ohta, K. Takada, L. Zhang, R. Ma, M. Osada, T. Sasaki, Adv. Mater. 18 (2006) 2226–2229.
[6] N. Ohta, K. Takada, I. Sakaguchi, L. Zhang, R. Ma, K. Fukuda, M. Osada, T. Sasaki, Electrochem. Commun. 9 (2007) 1486–1490.
[7] K. Takada, N. Ohta, L. Zhang, K. Fukuda, I. Sakaguchi, R. Ma, M. Osada, T. Sasaki, Solid State Ionics 179 (2008) 1333–1337.
[8] Y. Seino, T. Ota, K. Takada, J. Power Sources 196 (2011) 6488–6492.
[9] M. Ogawa, R. Kanda, K. Yoshida, T. Uemura, K. Harada, J. Power Sources 205 (2012) 487–490.
[10] N. Ota, N. Okuda, K. Emura, A. Yamakawa, SEI Tech. Rev. 61 (2006) 41–47.
[11] M. Ogawa, K. Yoshida, K. Harada, SEI Tech. Rev. 74 (2012) 88–90.
[12] A. Sakuda, A. Hayashi, T. Ohtomo, S. Hama, M. Tatsumisago, Electrochemistry 80 (2012) 839.
[13] F. Mizuno, A. Hayashi, K. Tadanaga, M. Tatsumisago, Adv. Mater. 17 (2005) 918.
[14] A. Sakuda, A. Hayashi, M. Tatsumisago, Chem. Mater. 22 (2010) 949.
[15] S. Scharner, W. Weppner, P. Schmid-Beurmann, J. Electrochem. Soc. 146 (1999) 857–861.
[16] A. Sakuda, H. Kitaura, A. Hayashi, K. Tadanaga, M. Tatsumisago, Electrochem. Solid-State Lett. 11 (2008) A1–A3.